Journal of Alloys and Compounds 509 (2011) 200–205

Contents lists available at ScienceDirect

Journal of Alloys and Compounds

journal homepage: www.elsevier.com/locate/jallcom

Pulsed laser deposition of transparent ZnO/MgO multilayers

Ajay Kaushal, Davinder Kaur*

Functional Nanomaterials Research Lab, Department of Physics and Center of Nanotechnology, Indian Institute of Technology Roorkee, Roorkee, India

ARTICLE INFO

Article history:
Received 27 February 2010
Received in revised form 9 September 2010
Accepted 18 September 2010
Available online 25 September 2010

Keywords:
ZnO/MgO multilayers
Nanorods
Pulsed laser deposition
Photoluminescence

ABSTRACT

We report on the structural, optical and electrical properties of ZnO/MgO multilayers grown by pulsed laser deposition technique. The film thickness of ZnO sublayer (t_{ZnO}) was found to have great impact on the properties of ZnO/MgO multilayers. Investigations reveal the structural phase transition from wurtzite phase to cubic phase with corresponding decrease in ZnO thickness. The optical transmittance of the multilayers is over 80% in the visible region and there is a gradual shift of absorption edge towards a longer wavelength with corresponding increase in ZnO sublayer thickness. Two absorption bands at around 400 nm and 270 nm were observed in the transmission spectra of ZnO/MgO multilayers for similar ZnO and MgO layer thickness, which has been ascribed to phase separation to hexagonal and cubic phases. The calculated optical band gap E_g shows a widening from 3.51 eV to 6.23 eV with corresponding decrease in ZnO sublayer thickness from 100 nm to 23 nm, which in turn leads to an increase in resistivity in ZnO/MgO multilayers. These results provide important information for the design and modeling of ZnO/MgO optoelectronic devices due to their adjustable bandgap energies.

1. Introduction

Multilayer deposition of oxide semiconductor thin films has attracted considerable and growing interest for functional device applications. In most of the cases these thin films showed enhanced or new physical properties, and sometimes combine the functional properties of two different materials. Recently, a great deal of research effort has been devoted to wide band gap semiconductors especially zinc oxide (ZnO) with direct band gap of 3.37 eV, high exciton binding energy of 60 meV and a large internal piezoelectric coefficient, making it useful in solar cells, light emitting diodes, gas sensing devices and transistors [1–5]. Its solid solution with MgO can produce higher band-gap ZnMgO alloys for potential applications in optoelectronic devices [6–8]. The ZnMgO alloy has been manifested as one of the most convenient material for realizing band gap modulation in ZnO based heterostructures because of its small lattice mismatch with ZnO and moreover growth conditions of these alloy layers are compatible to those of ZnO epitaxial layers. Bhattacharya et al. [9] have reported ZnMgO ternary alloys with a band gap of ~6 eV fabricated by multilayer deposition of ZnO/MgO layers on single crystal sapphire substrate.

Earlier we have reported ZnMgO alloy films having a band gap above 5 eV on quartz substrate by the pulsed laser deposition technique [10]. In the present study, transparent ZnO/MgO multilayers have been grown using pulsed laser deposition technique on quartz substrate. The effect of ZnO sublayer thickness (t_{ZnO}) on structural, electrical and optical properties of ZnO/MgO multilayers has been investigated systematically. A clear shift of the absorption edge as well as photoluminescence peak to higher energies with a decrease in the ZnO layer thickness was observed. In addition, the growth of ZnO–MgO nanorods with length to diameter average ratio of 15 has been reported. The tuning of band gap from 3.51 to 6.23 eV has been obtained in these highly oriented ZnO/MgO multilayers on quartz substrate inspite of large lattice mismatch between substrate and multilayers.

2. Experimental

ZnO/MgO multilayer thin films were grown on quartz substrate by PLD using a 25 mm diameter target. The KrF excimer laser with wavelength of 248 nm was used for deposition. The pulse repetition rate was kept at 10 Hz with laser fluence of about 2–3 J cm^{-2}. The targets were prepared by the solid state reaction method. The substrates were cleaned sequentially in acetone, methanol and de-ionized water prior to deposition. The target to substrate distance was kept at 40 mm. The deposition temperature was kept at 750 °C. Before ablation, the chamber was evacuated to a base pressure of 10^{-6} Torr, and then the pure oxygen was introduced and maintained at the optimized pressure. The oxygen pressure was varied in the range from 1 mTorr to 350 mTorr. Deposition parameters of ZnO/MgO multilayers are listed in Table 1. After the deposition, the films were cooled down naturally. The thickness of the films was measured using surface profilometer. The thickness of each single ZnO layer was varied in the range of 23–100 nm followed with the MgO host layer with constant thickness of 40 nm. The orientation and crystallinity of the films were studied using a Bruker diffractrometer of Cu K_α (1.54 Å) radiations in a θ–2θ geometry. The microstructure was studied using field emission scanning electron microscope (FESEM) (FEI Quanta 200M). To prevent the charge buildup during FESEM observations, samples were coated with gold. The film composition was conducted using energy dispersive X-ray analysis (EDAX). The resistivity of the films was measured by a four probe resistivity method using Keithley instruments at room tempera-

* Corresponding author. Tel.: +91 1332 285407; fax: +91 1332 273560.
E-mail address: dkaurfph@iitr.ernet.in (D. Kaur).

0925-8388/$ – see front matter © 2010 Elsevier B.V. All rights reserved.
doi:10.1016/j.jallcom.2010.09.077

Table 1
Optimized deposition parameters for ZnO/MgO multilayers.

Deposition technique	Pulsed laser deposition (PLD)
Laser	KrF excimer laser
Laser wavelength	248 nm
Laser energy	350 mJ
Laser fluence	2–3 J cm^2
Repetition rate	10 Hz
Target used	Zno and MgO (25 mm diameter)
Thickness variation (t_{ZnO}/t_{MgO})	t_{ZnO} = 23, 40, 59, 77 and 100 nm; t_{MgO} = 40 nm
Base pressure	1×10^{-6} Torr
Gas used	High purity oxygen (99.7%)
Background oxygen pressure	1 mTorr
Substrate	Quartz
Substrate temperature	750 °C
Target to substrate distance	40 mm

ture. The contacts over the samples were made by silver paint. Optical properties in the wavelength range of 200–800 nm were studied using Cary 5000 UV–VIS–NIR spectrometer.

3. Results and discussion

3.1. Structural properties

Fig. 1 shows the XRD pattern of ZnO/MgO multilayers of different ZnO sublayer thicknesses (t_{ZnO}) in the range of 23–100 nm. The thickness of MgO host layer was kept constant at 40 nm. XRD pattern reveals a structural deviation from single wurtzite to single cubic phase via mixed phase structure with decrease in ZnO sublayer thickness. It has been observed that ZnO sublayer of 59 nm thickness shows a single-wurtzite (0 0 2) oriented phase whereas the films with ZnO thickness of 23 nm show the cubic phase with preferred (1 1 1) direction. Mixed phase is observed for the equal sublayer and matrix thickness ($t_{ZnO} = t_{MgO} = 40$ nm). The observed phase transformation from wurtzite to cubic phase could be attributed to the increase of Mg/Zn ratio with decrease in ZnO sublayer thickness in ZnO/MgO multilayer thin films. Moreover, the

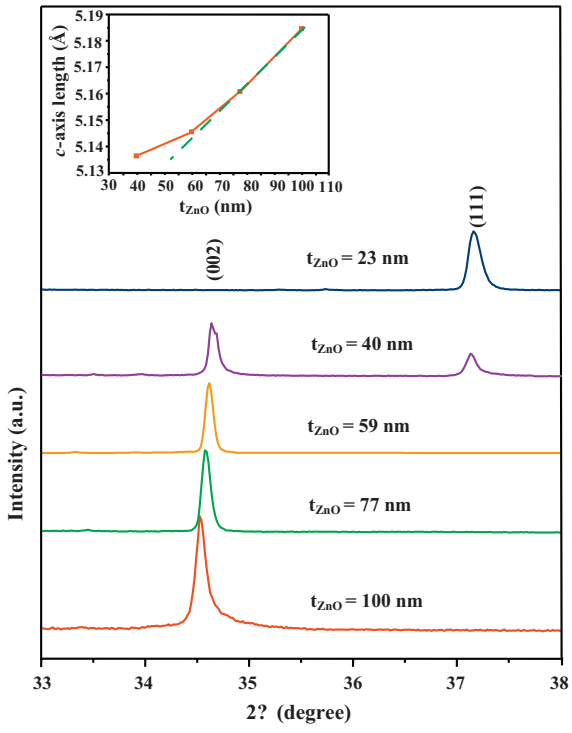

Fig. 1. XRD patterns of ZnO/MgO multilayers of different ZnO sublayer thicknesses. Inset shows the *c*-axis length variation with ZnO sublayer thickness.

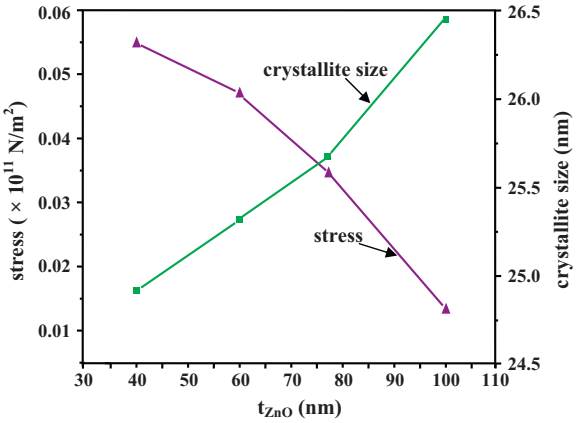

Fig. 2. Variation of crystallite size and stress with ZnO sublayer thickness in ZnO/MgO multilayers.

large angle between the nearest neighbour Zn–O bonds than that of Mg–O, leads to stronger interaction between the second nearest neighbour Mg–O bonds due to the stronger polarity of the Mg–O bonds, which results in deviation of crystal structure from wurtzite to cubic as the ratio of Mg/Zn is increased. XRD pattern also shows a slight shift of the diffraction peaks towards higher angle with decrease in ZnO sublayer thickness which manifests itself by the *c*-axis compression.

Inset of Fig. 1 shows the variation of *c*-axis lattice constant of ZnO/MgO multilayers of different ZnO sublayer thicknesses. The *c*-axis length calculated from the (0 0 2) diffraction peak decreases from 5.184 Å (t_{ZnO} = 100 nm), 5.161 Å (t_{ZnO} = 77 nm), 5.145 Å (t_{ZnO} = 59 nm) to 5.136 Å (t_{ZnO} = 40 nm) (Table 2). Since the ionic radius of Zn^{2+} (0.60 Å) is larger than that of Mg^{2+} (0.57 Å), the linear decrease of the *c*-axis lattice constant with decrease in ZnO sublayer thickness reveals the incorporation of Zn atoms into the cubic MgO lattice, which could be due to structural adjustment as the variation of lattice constant is related to the bond flex of anion and cation, radius difference of substitutional ion, and change of crystal structure. The *c*-axis length deviates from the linear fit, which could be due to presence of compensated defects or residual strain as reported by Ryoken et al. [11]. The observed value of the peak width broadening (FWHM) of the wurtzite (0 0 2) reflection was found to be 0.31° (t_{ZnO} = 100 nm), 0.32° (t_{ZnO} = 77 nm), 0.32° (t_{ZnO} = 59 nm) and 0.33° (t_{ZnO} = 40 nm). The increase of FWHM could be due to residual stress in the film. For hexagonal structure, the stress in the plane of the film can be calculated by using the following relation [12]:

$$\sigma = \left[2C_{13} - \frac{C_{33}(C_{11} + C_{12})}{C_{13}}\right] e_{zz} \quad (1)$$

and e_{zz} is the strain normal to the substrate calculated from the measured lattice constant by equation:

$$e_{zz} = \frac{(c - c_0)}{c_0} \quad (2)$$

where c is the lattice constant, c_0 is the corresponding bulk value (0.5206 nm), and C_{ij} are elastic stiffness constants $C_{11} = 2.1 \times 10^{11}$ N/m^2, $C_{33} = 2.1 \times 10^{11}$ N/m^2, $C_{12} = 1.2 \times 10^{11}$ N/m^2 and $C_{13} = 1.05 \times 10^{11}$ N/m^2 [13]. The numerical relation for the stress can be expressed as:

$$\sigma = -4.5 \times 10^{11} \frac{(c - c_0)}{c_0} \text{ N/m}^2 \quad (3)$$

The calculated results are shown in Table 2. The value of stress along *c*-axis oriented wurtzite films was found to increase from 0.0133×10^{11} to 0.0548×10^{11} N/m^2 with corresponding decrease

Table 2
Various calculated parameters of ZnO/MgO multilayers.

t_{ZnO}	Crystalline size (nm) along (0 0 2) peak	c-Axis length (Å)	Stress ($\times 10^{11}$ N/m^2)	Resistivity ρ (Ω cm)	E_g (eV) (transmission region)	E_g (absorption region)
100	26.43	5.184	0.0133	1.98×10^3	3.50	3.51
77	25.67	5.161	0.0337	3.36×10^3	3.57	3.61
59	25.30	5.145	0.0469	5.86×10^3	3.65	3.68
40	24.90	5.136	0.0548	1.09×10^4	4.21	4.25
23	–	–	–	1.36×10^4	6.19	6.23

in ZnO sublayer from 100 nm to 40 nm (Fig. 2). Further the crystallite size calculated from Scherrer formula [14] using FWHM values was found to decrease from 26.43 nm (t_{ZnO} = 100 nm), 25.67 nm (t_{ZnO} = 77 nm), 25.3 nm (t_{ZnO} = 59 nm) to 24.9 nm (t_{ZnO} = 40 nm) as shown in Fig. 2.

Fig. 3(a)–(e) shows the FESEM images of films with different ZnO sublayer thicknesses of t_{ZnO} = 100, 77, 59, 40 and 23 nm, respectively. FESEM images reveal nanorod like structure of micrometer length with an average diameter of 70 nm for the film with equal ZnO and MgO layer thickness (Fig. 3(d)). The average length to

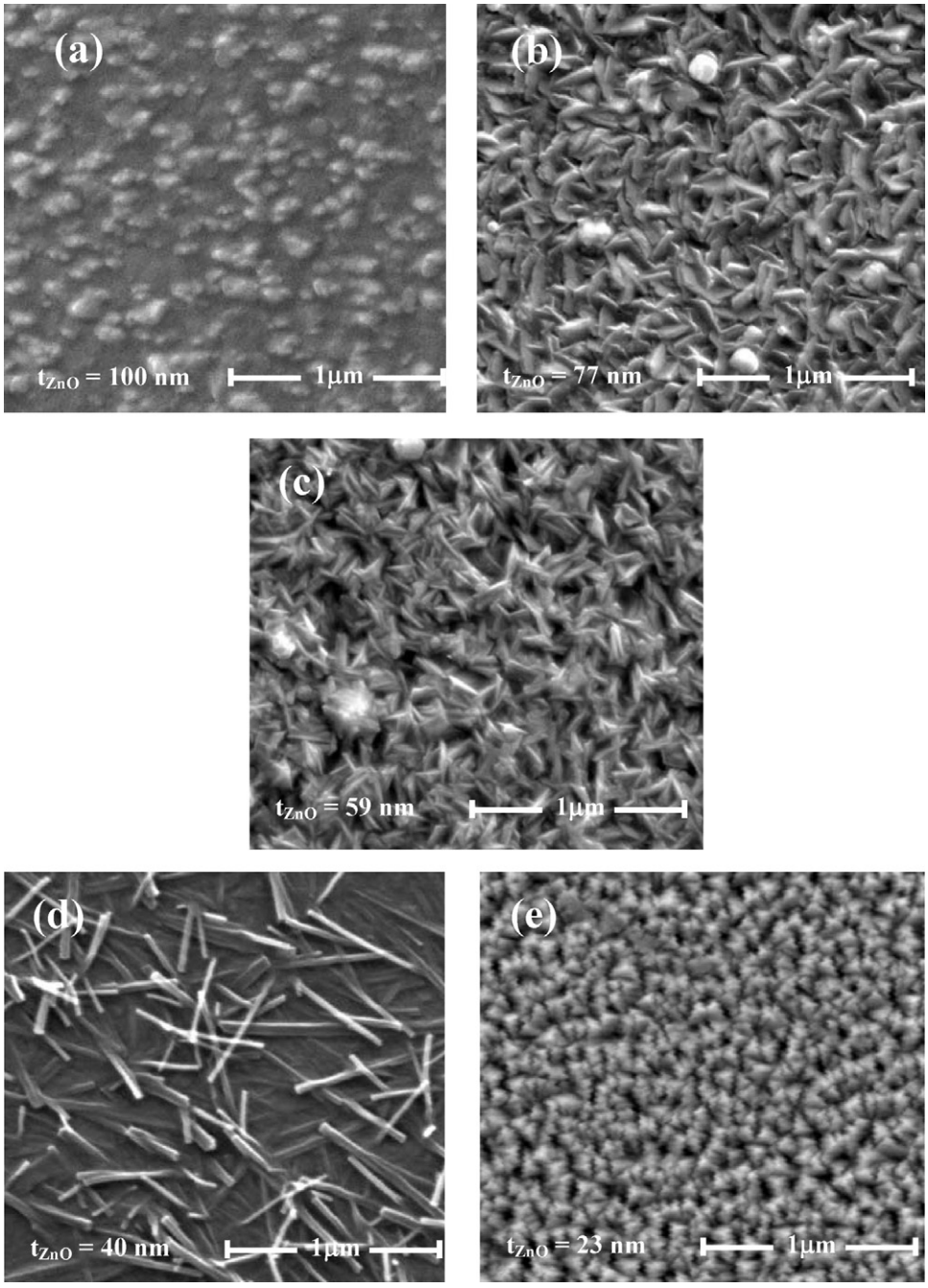

Fig. 3. FESEM images of ZnO/MgO multilayers of different ZnO sublayer thicknesses.

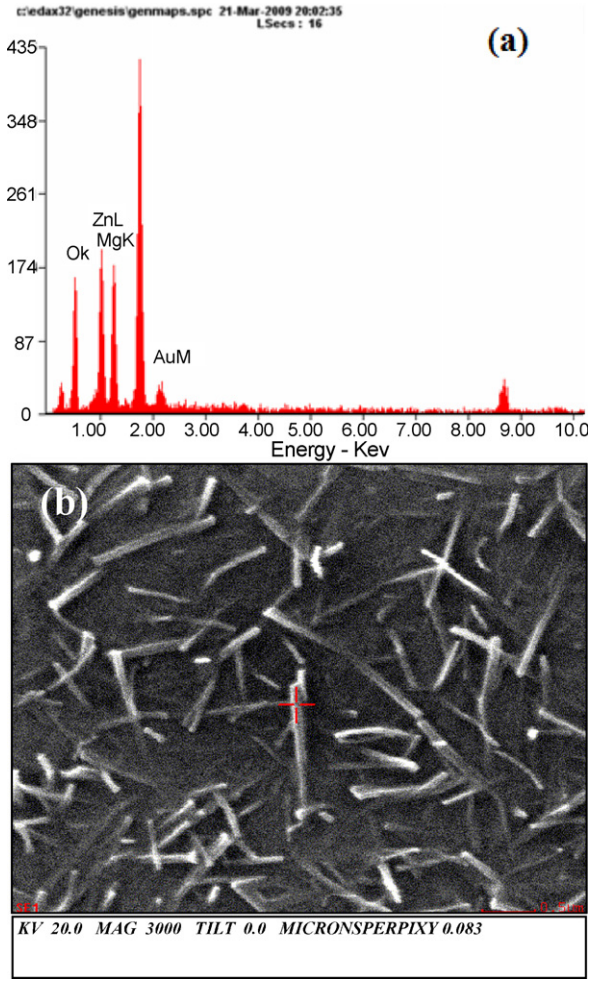

Fig. 4. (a) EDAX pattern of the ZnMgO nanorods and (b) corresponding selected nanorod in FESEM image.

diameter ratio of nanorods was found to be 15. The observed nanorods were randomly oriented which could be due to lack of lattice compatibility between the quartz surface and ZnO/MgO multilayers. Chang et al. [15] and Heo et al. [16] have reported maximum Mg content of 17% in MOCVD and MBE deposited ZnMgO nanorods. However in our case, we observed ZnMgO nanorods with Mg content up to 35% giving rise to large band gap tuning which prospects its application in solar blind photodetectors. The films with ZnO sublayer thickness of 59 and 77 nm show a continuous film with columnar shaped grains (Fig. 3(b and c)). When ZnO sublayer thickness decreases to 23 nm i.e. becomes less than MgO host sublayer thickness, the film shows the formation of smaller distinct independent grain morphology with some ridges along the pyramids (Fig. 3(e)). The films became more regular with an equiaxial shaped grains of an average grain size around 70 nm, when ZnO sublayer thickness becomes less than MgO host sublayer. In case of ZnO/MgO multilayers with $t_{ZnO} = t_{MgO} = 40$ nm, the host MgO matrix creates nucleation site for the ZnO sublayer and may serve as seeds for the growth of ZnMgO nanorods. The presence of Mg in the ZnMgO nanorods was confirmed by EDAX measurement. Fig. 4(a) shows the EDAX pattern of the selected nanorod as shown in the corresponding FESEM image (Fig. 4(b)). EDAX pattern gives the 44.20 and 34.79 wt% of Zn and Mg element, respectively, which shows an evidence of the presence of both Zn as well as Mg in the nanorods.

3.2. Optical properties

3.2.1. Determination of optical band gap

Fig. 5 shows the optical transmission spectra of ZnO/MgO multilayers of different ZnO sublayer thicknesses. All the films were found to be highly transparent with an average transmittance of about 80%. It was observed that the transmission of the films decreases from 84% to 78% and there is a gradual shift of ultraviolet cutoff towards longer wavelength with corresponding increase in ZnO sublayer thickness from 23 nm to 100 nm. At low value of ZnO sublayer thickness ($t_{ZnO} = 23$ nm and 40 nm), the films were transparent with an average transmittance of 84% in the visible range of the electromagnetic spectra and presented a sharp ultraviolet cutoff. For $t_{ZnO} = 40$ nm, two absorption bands at around 400 nm and 270 nm were observed in the transmission spectra of ZnO/MgO thin films, which could be attributed to phase separation into hexagonal and cubic phases. These absorptions were ascribed to charge transfer between donor and acceptor ionization level located within the band gap of the ZnO and MgO [17,18]. The optical absorption coefficient α was calculated from the following relation [19]:

$$T = \frac{(1-R)^2 \exp(-\alpha t)}{1 - R^2 \exp(-2\alpha t)}$$

where R and T are the spectral reflectance and transmittance and t is the film thickness. For greater optical density ($\alpha t > 1$), the interference effects due to internal reflections as well as reflectance at normal incidence are negligible, and the previous equation can be approximated as

$$T \approx \exp(-\alpha t)$$

The optical absorption coefficient α is given by an approximate formula,

$$\alpha = -\frac{1}{t} \ln T$$

where t is the film thickness and T is the measured transmittance. The direct band gap of the films was calculated using the Tauc relationship as follows:

$$\alpha h\upsilon = A(h\upsilon - E_g)^n$$

where α is the absorption coefficient, A is a constant, h is the Planck's constant, υ is the photon frequency, E_g is the energy band gap and n is 1/2 for direct band gap semiconductor. An extrapolation of the linear region of a plot of $(\alpha h\upsilon)^{1/n}$ on the y-axis vs. photon energy

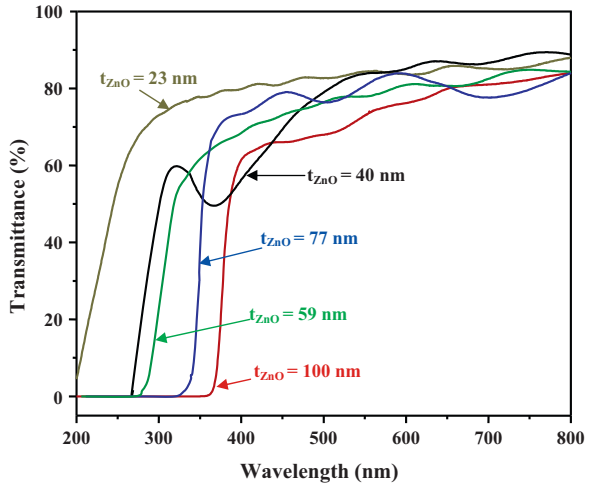

Fig. 5. Transmission spectra of ZnO/MgO multilayers of different ZnO sublayer thicknesses.

($h\upsilon$) on the x-axis gave the value of the energy band gap E_g. Since $E_g = h\upsilon$ when $(\alpha h\upsilon)^2 = 0$, here the direct band gap of the ZnO/MgO multilayer thin films was evaluated by extrapolating the straight line part of the curves $(\alpha h\upsilon)^2 = 0$ as shown in Fig. 6. The inset shows the corresponding evaluated band-gap values emphasizing phase transition. The value of band gap was found to increase from 3.51 eV to 6.23 eV with corresponding decrease in t_{ZnO} from 100 nm to 23 nm, as shown in inset of Fig. 6. An abrupt change in band-gap value is observed at $t_{ZnO} = 40$ nm which could be attributed to phase transition from hexagonal to cubic-phase. Zhang et al. [20] have reported maximum band gap tuning of 3.78 eV in ZnMgO nanorods, however in present study a band gap tuning of 4.25 eV in ZnMgO nanorods has been observed. The blue shift in band gap is due to the modulation of bandgap caused by decrease of ZnO thickness in ZnO/MgO multilayers indicative of achievement of bandgap engineering in ZnMgO nanostructures. There is no evidence of quantum size effect for the obtained nanorods, since their diameters are about 70 nm.

The refractive index (n) of multilayers was estimated from the transmission spectrum by using the envelope method, and the following expression was used to calculate the refractive index:

$$n = [N + (N^2 - {n_0}^2{n_1}^2)^{1/2}]^{1/2}$$

where

$$N = \frac{{n_0}^2 + {n_1}^2}{2} + 2n_0n_1\frac{T_{max} - T_{min}}{T_{max}T_{min}}$$

and n_0 and n_1 (1.46 in our case) are the refractive index of air and substrate, respectively. T_{max} and T_{min} are maximum and minimum transmittance values at the same wavelength. Fig. 7(a) represents the refractive indices (n) calculated at different wavelengths for ZnO/MgO films of different ZnO sublayer thicknesses. The average value of refractive indices (n) evaluated at different wavelengths was found to decrease with corresponding decrease in ZnO sublayer thickness from 100 nm to 23 nm. In general, the refractive indices of the oxides were related to the dispersion energy parameters E_d and E_o, using the single term Sellmeier dispersion relation [21,22]:

$$n^2 - 1 = \frac{E_dE_o}{(E_0^2 - h^2\nu^2)} \quad (4)$$

where $h\nu$ is the photon energy and E_o is the single oscillator energy. The parameter E_d is the dispersion energy, which is a measure of the strength of interband optical transitions. The dispersion plays an important role in the research for optical materials, because

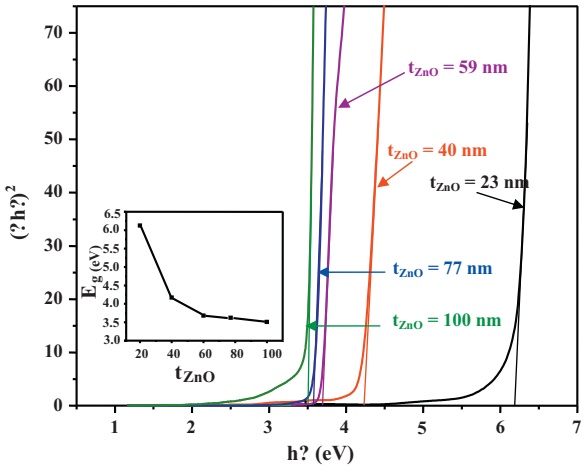

Fig. 6. $(\alpha h\upsilon)^2$ vs. $h\upsilon$ plots of ZnO/MgO multilayers of different ZnO sublayer thicknesses. Inset shows the calculated bandgap variation with ZnO sublayer thickness.

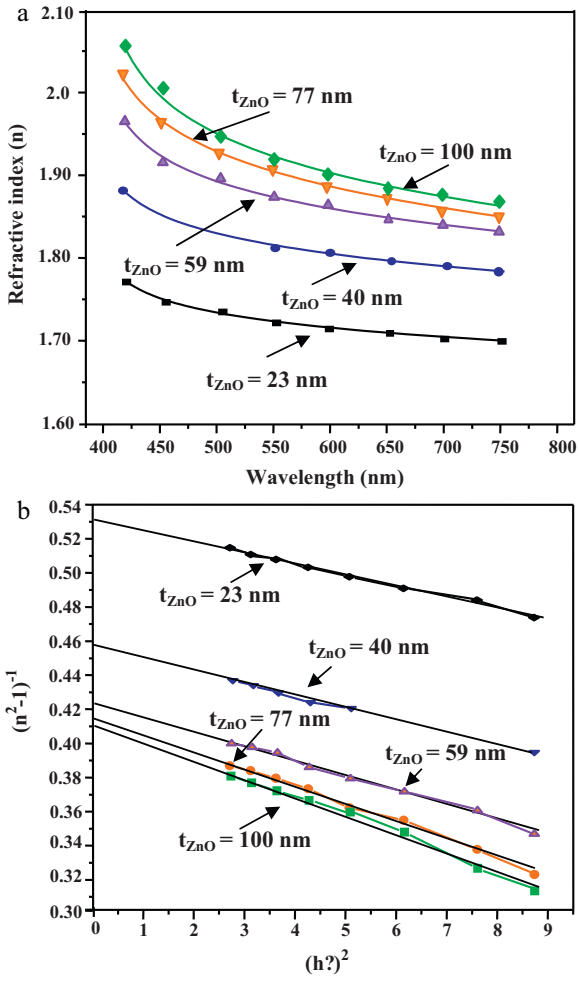

Fig. 7. (a) Calculated refractive index and (b) $(n^2 - 1)^{-1}$ vs. $(h\nu)^2$ variation of ZnO/MgO multilayers of different ZnO sublayer thicknesses.

it is a significant factor in optical communication. The oscillator energy E_o is an average of the optical band gap, E_g, and can be obtained from experimental verification of Eq. (4) by plotting $(n^2 - 1)^{-1}$ vs. $(h\nu)^2$ as illustrated in Fig. 7(b). The variation yields a straight line having slope $(E_oE_d)^{-1}$ and the intercept with the vertical axis equal to (E_o/E_d). The optical band gap values were calculated from Wemple–Didomenico dispersion parameters using relation $E_g \approx E_o/2$ [23,24] and are in consistence with those calculated by Tauc method. The calculated values of optical band gap are listed in Table 2. The small difference between the bandgap values calculated from two different methods is attributed to the calculation in different regions of the spectrum. In case of Wemple–Didomenico model, the values of the band gap E_g were calculated in the transparent region of the spectrum (depending upon the values of n) while, in Tauc method the band gap was calculated in the absorption region of the spectrum.

3.2.2. Photoluminescence

Fig. 8 shows the photoluminescence (PL) excitation and emission spectra of the films at room temperature. The excitation spectra showed two prominent peaks, one around 212 nm (5.86 eV) and other around 240 nm (5.18 eV). The position of excitation at 240 nm remained almost same for all the samples. The PL curve exhibits peak near ultraviolet region which shifts towards lower wavelength with decrease in ZnO sublayer thickness. The emission peak was tuned from 421 nm to 377 nm with corresponding decrease in ZnO sublayer thickness from 100 nm to 23 nm. The

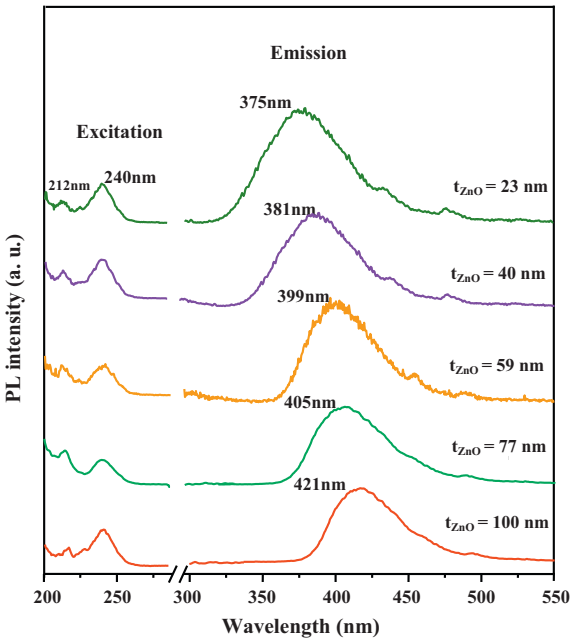

Fig. 8. PL spectra of ZnO/MgO multilayers of different ZnO sublayer thicknesses.

observed blue shift could be due to the introduction of more defects as MgO tends to form solid solution at lower value of ZnO sublayer thickness due to the electronegativity and ionic radius difference between Zn and Mg. As a result, the bound excitons increase with decrease in t_{ZnO} as Mg/Zn ratio increases and subsequent radiative recombination of these excitons lead to a blue shift. A slight broadening with decrease in t_{ZnO} in ZnO/MgO multilayers has also been found which is believed to be due to fluctuations in the compound, where localized excitons experience a different Coulomb potential depending on the arrangement of the substitutional element [25].

3.3. Electrical resistivity

Fig. 9 shows the variation of resistivity as a function of ZnO sublayer thickness. The values of resistivity of wurtzite films were found to be of the order of $10^3\ \Omega$ cm whereas values of resistivity of cubic films were of the order of $10^4\ \Omega$ cm (Table 2). The resistivity of ZnO/MgO films is related to ZnO sublayer thickness, intrinsic defects (e.g. Zn interstitials and O vacancies) and various scattering centers. Mg/Zn ratio increases with decrease in ZnO sublayer thickness in ZnO/MgO multilayer films, which results in (i) suppression of ZnO tendency to form interstitial metal atom and oxygen

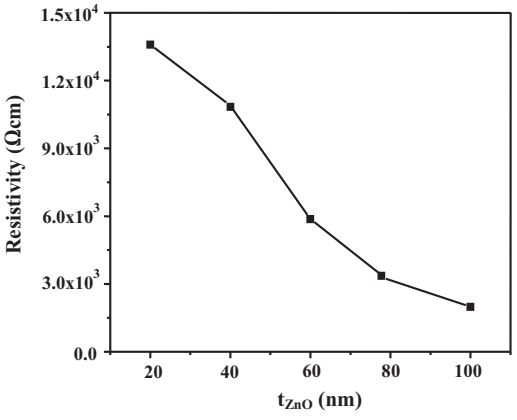

Fig. 9. Variation of resistivity as a function of ZnO sublayer thickness.

vacancy defects; (ii) increase in band gap as the MgO (6.67 eV) has larger band gap compared to ZnO (3.37 eV). Thus, the decrease in oxygen vacancy defects and the increase in bandgap, both make contribution to an increase in resistivity of ZnO/MgO multilayers.

4. Conclusion

In summary, ZnO–MgO multilayers have been grown successfully on quartz substrate by pulsed laser deposition technique. The thickness of ZnO sublayer was found to have great impact on the structural features and optical properties of these multilayers. Formation of ZnMgO nanorods was observed with Mg content up to 35% for equal ZnO and MgO sublayer thickness of 40 nm. The optical band gap tuning in ZnO/MgO multilayers was investigated by evaluating them in both transparent as well as in absorption regions of the transmission spectra. The optical band gap was calculated in terms of Tauc and Wemple–Didomenico model. The band gap values obtained from Wemple–Didomenico model were in agreement with those determined from Tauc method. The optical band gap tuning from 3.51 eV to 6.23 eV was observed with corresponding decrease in ZnO sublayer thickness from 100 nm to 23 nm. The indices of refraction below the band gap were determined by Swanepoel's method and were well described by Sellmeier relation. Decrease in ZnO sublayer thickness in ZnO/MgO multilayers leads to an increase in band gap and electrical resistivity. These results prospect ZnO/MgO multilayers for potential application in optoelectronic devices.

Acknowledgement

The financial support provided by Ministry of Communications and Information Technology (MIT), India under Nanotechnology Initiative Program with reference no. 20(11)/2007-VCND is highly acknowledged.

References

[1] S. Major, K.L. Chopra, Sol. Energy Mater. 17 (1988) 319.
[2] K.L. Chopra, S. Major, D.K. Panday, Thin Solid Films 102 (1983) 1.
[3] S.J. pearton, D.P. Norton, Y.W. Heo, T. Steiner, Prog. Mater. Sci. 50 (2005) 293.
[4] P. Bhattacharya, R.R. Das, R.S. Katiyar, Appl. Phys. Lett. 83 (2003) 2010.
[5] B. Yang, A. Kumar, P. Feng, R.S. Katiyar, Appl. Phys. Lett. 92 (2008) 233112.
[6] M.X. Qiu, Z.Z. Ye, H.P. He, Y.Z. Zhang, X.Q. Gu, L.P. Zhu, B.H. Zhao, Appl. Phys. Lett. 75 (1999) 980.
[7] T. Makino, Y. Segawa, M. Kawasaki, A. Ohtomo, R. Shiroki, K. Tamura, T. Yasuda, H. Koinuma, Appl. Phys. Lett. 78 (2001) 1237.
[8] X. Zhang, X.M. Li, T.L. Chen, C.Y. Zhang, W.D. Yu, Appl. Phys. Lett. 87 (2005) 092101.
[9] P. Battacharya, R.R. Das, R.S. Katiyar, Thin Solid Films 447 (2003) 564.
[10] A. Kaushal, D. Kaur, Sol. Energy Mater. Sol. Cells 93 (2009) 193.
[11] H. Ryoken, N. Ohasahi, I. Sakaguchi, Y. Adachi, S. Hishita, H. Haneda, J. Cryst. Growth 287 (2006) 134.
[12] S. Maniv, W.D. Westwood, E. Colombini, J. Vac. Sci. Technol. 20 (1982) 162.
[13] K.H. Hellwege, A.M. Hellwege (Eds.), Landolt–Bornstein Series, vol. 2, Springer, Berlin, 1969, p. 58.
[14] B.D. Cullity, Elements of X-ray Diffraction, Addison-Wesley, 1970.
[15] Y.S. Chang, C.T. Chien, C.W. Chen, T.Y. Chu, H.H. Chiang, C.H. Ku, J.J. Wu, C.S. Lin, L.C. Chen, K.H. Chen, J. Appl. Phys. 101 (2007) 033502.
[16] Y.W. Heo, M. Kaufman, K. Pruessner, D.P. Norton, F. Ren, M.F. Chisholm, P.H. Fleming, Solid State Electron. 47 (2003) 2269.
[17] I. Takeuchi, W. Yang, K.S. Chang, M.A. Aronova, T. Venkatesan, R.D. Vispute, L.A. Bendersky, J. Appl. Phys. 94 (2003) 7336.
[18] C.H. Bates, W.B. White, R. Roy, J. Inorg. Nucl. Chem. 28 (1966) 397.
[19] Z.S. El Mandouh, M.S. Selim, Thin Solid Films 371 (2002) 259.
[20] Y.Z. Zhang, J.G. Lu, Z.Z. Ye, Y.J. Zeng, L.P. Zhu, J.Y. Huang, J. Phys. D: Appl. Phys. 40 (2007) 3490.
[21] M. Didomenico, S.H. Wemple, J. Appl. Phys. 40 (1969) 720.
[22] S.H. Wemple, M. Didomenico, Phys. Rev. B 3 (1971) 1338.
[23] E. Marquez, A.M. Bernal-Oliva, J.M. Gonzalez-Leal, R. Pricto-Alcon, A. Ledesma, R. Jimenez-Garay, I. Martil, Mater. Chem. Phys. 60 (1999) 231.
[24] E. Marquez, P. Nagels, J.M. Gonzalez-Leal, A.M. Bernal Oliva, E. Sleeckx, R. Callaerts, Vacuum 52 (1999) 55.
[25] W.I. Park, G.C. Yi, H.M. Jang, Appl. Phys. Lett. 79 (2001) 2022.